

PEGylated Silk Fibroin Nanoparticles for Oral Antibiotic Delivery: Insights into Drug–Carrier Interactions and Process Greenness

Duy Toan Pham, Thi Truc Dao Le, Ngoc Yen Nguyen, Chong Kim Thien Duc, Nguyen Trong Tuan, Huynh Vu Thanh Luong, Quyen Thi Bich Tran, Manh Quan Nguyen, and Bui Thi Phuong Thuy*



Cite This: *ACS Omega* 2025, 10, 11627–11641



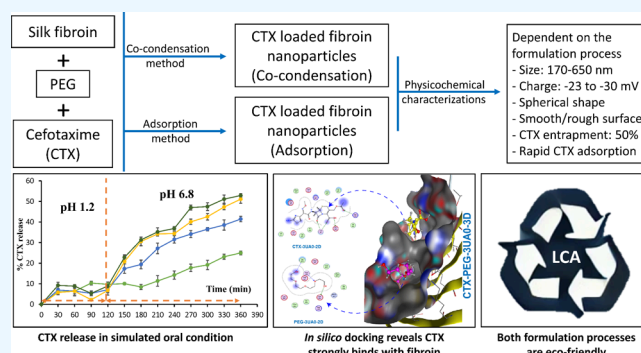
Read Online

ACCESS |

Metrics & More

Article Recommendations

ABSTRACT: Insights into antibiotic–carrier interactions in the silk-fibroin-based nanoparticles and considerations on the formulation process greenness are limited. Hence, this work developed and characterized polyethylene glycol-functionalized silk fibroin nanoparticles for oral delivery of cefotaxime (PEG/SFPs-CTX), with a focus on the *in silico* simulations and process greenness. The particles were formulated by the two methods of co-condensation and adsorption. Dependent on the processes, the particles possessed spherical shape, smooth/rough surfaces, nanosize (170–650 nm), negative charge (−23 to −30 mV), and drug entrapment efficiency of ~50%. The system rapidly absorbed the drug within 30 min, followed second-order kinetics, and significantly controlled the drug release rate in the simulated gastrointestinal system, which could bypass the stomach acidic pH. Interestingly, *in silico* docking revealed that CTX mostly bound strongly and noncovalently with fibroin, particularly at glutamic acid, via hydrogen bonds, van der Waals forces, and π – π interactions, while PEG enhanced the stability of the system. Molecular dynamics simulations confirmed the complex's stability under physiological conditions. Lastly, life cycle assessment analysis showed that both formulation methods were environmental friendly, with limited impacts on the ecosystem, and the adsorption method was “greener” than the co-condensation method.



1. INTRODUCTION

The oral route is among the most common methods of pharmaceutical delivery because of its safety, patient compliance, and low production costs.¹ Nevertheless, conventional medications, such as capsules and tablets, release active components uncontrollably, resulting in unwanted drug degradations in the gastrointestinal system.² This issue is even more crucial for antibiotics since most antibiotics have low oral bioavailability mainly due to their complex molecular/chemical structure and instability in the acidic environment of the stomach. Additionally, intravenous administration of antibiotics could extend hospitalization, which increases healthcare costs and the risk of healthcare-associated adverse events such as hospital-acquired infections.³ The recent so-called outpatient parenteral antimicrobial therapy (OPAT) program, which enables patients to do intravenous injection at home, however, possesses various disadvantages, namely, the complications from the self-administration devices, antibiotic side effects and instability, and patient rejection and non-adherence.³ Thus, efforts have been made to improve the oral delivery of antibiotics, possibly by encapsulation in a drug delivery system.

Drug delivery systems such as nanoparticles, commonly employing a biomaterial as carrier, could load and control the drug release favorably, thus avoiding the drug degradation in the stomach.^{4,5} Moreover, the drug–carrier interactions might alter the drug physicochemical properties, making it more absorbable in the small intestine. Regarding the biomaterials used to formulate nanoparticles, silk fibroin has gained increasing interests.⁶ Fibroin is an amphiphilic polymer generated from the cocoon of the silkworm *Bombyx mori*, which is highly biocompatible, biodegradable, and nontoxic.^{7–9} Silk fibroin nanoparticles (SFPs) have been utilized extensively to deliver various drugs/extracts, namely, paclitaxel,¹⁰ amphotericin B,¹¹ different drugs belonging to four biopharmaceutics classification system (BCS) classes,^{12,13} *Wedelia trilobata* L. extract,¹⁴ and guava extract.¹⁵ SFPs are stable throughout a wide pH range of 5–14 and remain stable at pH

Received: February 5, 2025

Revised: March 2, 2025

Accepted: March 7, 2025

Published: March 14, 2025



< 5 at 0.2% concentration, making them ideal for oral drug administration.¹⁶ Furthermore, SFPs could attach to the gastrointestinal mucosa or intestinal epithelial cells and be endocytosed, making the encapsulated compounds reach the bloodstream easily.¹⁷

However, SFPs are prone to aggregations and accumulations;¹⁸ thus, the functionalization of SFPs with polymers such as polyethylene glycol (PEG) (PEG/SFPs), also known as PEGylation, is commonly employed.^{19–22} PEG is an amphiphilic polymer, soluble in distilled water,²³ and is generally used for the chemical modification of natural and synthetic macromolecules in biological applications.²⁴ Chemically active hydroxyl groups at both ends of the PEG chain could interact with functional groups of fibroin like amine, carboxylic, ester, and hydroxyl.²⁵ Furthermore, the pharmacokinetic characteristics of peptides, proteins, hydrophobic polymers, medicines, and nanoparticles can be considerably enhanced when being PEGylated.²⁶ As a result, PEG has emerged as the most widely utilized polymer in biomedical research, with the FDA having authorized 20 PEGylated liposomes or RNA liposomes for clinical use.²⁷

Cefotaxime (CTX) is a broad-spectrum third-generation cephalosporin antibiotic with low toxicity but limited oral bioavailability.^{28,29} CTX is active against both Gram-negative and Gram-positive bacteria and is used in treating infections of the respiratory tract and skin.^{30–32} Nevertheless, CTX is not available as an oral medication due to its large and hydrophilic structure, making it difficult to cross the lipid membranes of the intestinal epithelium for absorption into the systemic circulation.³³ Moreover, CTX is unstable in the acidic environment of the stomach, which leads to significant degradation before it can be absorbed.³⁴ Both of these issues could be overcome by encapsulating CTX in PEGylated SFPs (PEG/SFPs-CTX).

Additionally, as previously mentioned, various studies have developed SFPs for drug delivery. However, limited information has been reported on the in-depth interactions and chemical binding mechanisms of drug carriers (i.e., between CTX, fibroin, and PEG), especially in physiological conditions. Therefore, in this present work, *in silico* docking and molecular dynamics (MD) simulations were used to study this interaction with the fibroin model 3UA0.³⁵ Docking identified binding sites, types of interactions (i.e., hydrogen bonds, van der Waals, and π - π interactions), and the stability of the complex.^{36,37} On the other hand, MD provided insights into the stability and flexibility of the complex under various physiological conditions, such as pH, temperature, and aqueous environments.³⁸ This combined approach assessed the compatibility and efficacy of PEG/SFPs-CTX, supporting the design of nanocarriers to improve CTX bioavailability and therapeutic efficacy.

Another issue to note is that most nanoparticle formulation methods/processes only focus on the efficacy and optimal products but do not tackle the environmental concern. On the one hand, nanoparticles themselves cause noteworthy threats to humans and the environment, including cell death, DNA damage, and soil and water pollutions.³⁹ On the other hand, the processes of making nanoparticles pose even more critical damages since they often utilize harmful organic solvents, equipment with high electricity usages, and toxic reagents/byproducts.⁴⁰ Thus, critical concerns should be focused on the green factors of the nanoparticle formulation processes. One of the most widely used techniques for assessing the environ-

mental effects of these processes is life cycle assessment (LCA). This approach is crucial for advancing sustainable development because it helps firms analyze, assess, and improve processes by identifying environmental impact indicators, including ozone depletion, acidification, climate change, and human toxicity.⁴¹ Nevertheless, there is currently little use of LCA in SFP formulation processes.

Ultimately, this research aimed to develop and characterize PEG/SFPs, encapsulating CTX, for oral delivery by two distinct methods of co-condensation and adsorption. Non-functionalized SFPs were also formulated as a reference. The selection of these methods was based on their regularity in nanoparticle formulations, efficiency in drug incorporation, process simplicity, and overall environmental impact. Co-condensation was chosen for its ability to incorporate the drug during particle formation, potentially enhancing uniformity and stability, while adsorption was selected as a postformulation method to minimize solvent use and preserve the native properties of both the drug and carrier system. Therefore, although both methods are commonly employed, they may exhibit substantial differences in their environmental impacts, which should be considered. Besides evaluating the general particle physicochemical properties (i.e., size, zeta potential, shape, morphology, drug entrapment efficiency, chemical interactions, and CTX release profiles in the simulated gastrointestinal tract), the work deeply focused on the CTX molecular interactions with fibroin and PEG using *in silico* docking and MD simulation. More importantly, LCA was used to evaluate the greenness of the two utilized methods in the study to select a more environmentally friendly method while still ensuring a high nanoparticle generation efficiency.

2. MATERIALS AND METHODS

2.1. Materials. Silkworm cocoons from *Bombyx mori* were obtained from Phuong Dinh commune, Truc Ninh district, Nam Dinh province, Vietnam. CTX, in the form of sodium salt, was purchased from the Long Chau pharmaceutical system in Can Tho city, Vietnam. Sigma-Aldrich supplied PEG 1450. The Cemaco company provided absolute ethanol (EtOH, 99.5%), calcium chloride (CaCl_2), calcium nitrate ($\text{Ca}(\text{NO}_3)_2$), and sodium carbonate (Na_2CO_3).

2.2. Fibroin Extraction. The silk fibroin extraction technique was done similarly to the work by Pham et al.¹³ Specifically, sericin was removed by heating 5 g of dried cocoons in 200 mL of 0.5% Na_2CO_3 for 1 h at 80 °C. The finished silk fiber was washed with distilled water and air-dried. After drying, it was poured into a mixture of CaCl_2 , $\text{Ca}(\text{NO}_3)_2$, H_2O , and EtOH at a mass ratio of 30:45:5:20 and microwaved for 2 min to generate a clear solution. The solution was then dialyzed against distilled water using a cellulose filter (10,000 MWCO) at room temperature for 4 days. Finally, contaminants were removed from the solution by centrifugation at 6000 rpm for 30 min. The purified solution was freeze-dried to yield fibroin powder.

2.3. Formulation of the Blank SFPs and PEG/SFPs. The blank SFPs and PEG/SFPs were created by using the simple one-pot condensation method. Briefly, to 1 mL of the 1/2% fibroin aqueous solution, 1 mL of the PEG aqueous solution (0 (i.e., 1 mL water, for the nonfunctionalized formula), 1, or 2%) was added. The final concentrations of fibroin and PEG in the mixture were 0.5/1 and 0/0.5/1%; thus, the formulas were abbreviated as SFPs-0.5, SFPs-1, PEG/SFPs-0.5, and PEG/SFPs-1, respectively. Then, 10 mL of

absolute EtOH was slowly added to the mixtures. The spontaneously formed particles were then collected by centrifuging at 6000 rpm for 10 min. Finally, the supernatant was discarded, and the particles were washed with distilled water thrice by centrifugation (6000 rpm, 10 min).

2.4. Preparation of the SFPs-CTX and PEG/SFPs-CTX.

To compare the product properties and the process greenness, two distinct methods were used to prepare SFPs-CTX and PEG/SFPs-CTX, namely, the co-condensation and the adsorption method.

$$EE\% = \frac{\text{initial amount of CTX(1 mg)} - \text{amount of CTX in supernatant}}{\text{initial amount of CTX(1 mg)}} \times 100(\%) \quad (1)$$

Adsorption Method. For this method, the blank particles were first formulated as described in Section 2.3 and redispersed in 50 mL of water containing 1 mg of CTX (final concentration of 20 $\mu\text{g/mL}$). The adsorption was carried out for 4 h under gentle stirring. Every 30 min, 2 mL of the dispersion was withdrawn, and the aspirates were UV–vis analyzed to determine the remaining drug concentration and the percentage of adsorbed CTX at each time point. After the adsorption duration, the particles were recovered by centrifuging the dispersion at 6000 rpm for 10 min. Finally, the particles were washed with distilled water thrice by centrifugation (6000 rpm, 10 min). To describe the adsorption process, general thermodynamic models were employed (Table 1).

Table 1. Models Used to Calculate the CTX Adsorption and Release Processes

adsorption model	equation	parameter
Dubinin–Radushkevich (D–R)	$\ln q_e = \ln q_m - \beta \epsilon^2$ $\epsilon = RT \ln \left(1 + \frac{1}{C_e} \right)$ $E = \frac{1}{\sqrt{2\beta}}$	β : adsorption energy constant (mol^2/J); ϵ : Polanyi potential energy; q_m : maximum adsorption capacity (mg/g); q_i : adsorption capacity at equilibrium time and at time t (mg/g); k_1 : apparent first-order (1/min); k_2 : second-order adsorption rate constant ($\text{g/mg}\cdot\text{min}$)
pseudo-first-order kinetics	$\ln(q_e - q_t) = \ln(q_e) - k_1 t$	
pseudo-second-order kinetics	$\frac{t}{q_t} = \frac{1}{k_2 q_e^2} + \frac{t}{q_e}$	
release model	equation	parameter
zero-order kinetic	$M_t = M_0 + k_0 t$	M_0 : initial amount; M_t : release amount at the time point t ; k_0 , k_1 , k_H , k_{HC} , and k_{KP} : the release constants of the zero-order, first-order, Higuchi, Hixson–Crowell, and Korsmeyer–Peppas models
first-order kinetic	$\ln(M_t) = \ln(M_0) - k_1 t$	
Higuchi	$M_t = k_H t^{1/2}$	
Hixson–Crowell	$M_t^{1/3} = M_0^{1/3} - k_{HC} t$	
Korsmeyer–Peppas	$\frac{M_t}{M_0} = k_{KP} t^n$	

2.5. Particle Characterizations. The particles were characterized in terms of general properties of size, charge (zeta potential), shape, morphology, chemical interactions, crystallinity, and *in vitro* CTX release in simulated oral condition.

Particle Size and Charge. The average size of the particles and size distribution (polydispersity index) were assessed using a MicroTrac S3500 analyzer by the dynamic light scattering (DLS) technique. The samples were dispersed in 5 mL of

Co-condensation Method. For this method, the SFPs-CTX and PEG/SFPs-CTX were prepared similarly to those of the blank particles (Section 2.3). The CTX powder (1 mg) was dissolved in the aqueous phases containing fibroin with and without PEG. All other formulation steps were conducted as described in Section 2.3. The CTX concentration in the supernatant, after the final centrifugation step, was determined using a Jasco V730 spectrophotometer at a wavelength of 234 nm and calculated using a calibration curve ($y = 0.0939x - 0.008$ ($R^2 = 0.9996$)). The CTX entrapment efficiency (EE%) was determined using eq 1.

distilled water, homogenized using a Mison ultrasonicator for 20 min, and measured at 25 $^{\circ}\text{C}$ with a fixed angle of 90 $^{\circ}$ following the machine instructions. The particle charge was also measured similarly to that of the size utilizing the phase analysis light scattering (PALS) technique.

Particle Morphology. The particle shape and morphology were examined with a scanning electron microscope (SEM) (Carl Zeiss, Germany). The particles were redispersed in water to a count rate of 400 kcps (estimated using the DLS method). The dispersions were then dropped and immobilized on a carbon disc mounted on a metal substrate coated with a 10 nm layer of gold, which were analyzed using SEM.

Chemical Interactions and Crystallinity. The structure and interactions between CTX, fibroin, and PEG in the particles were assessed using Fourier-transform infrared spectroscopy (FTIR), X-ray diffractometry (XRD), and differential scanning calorimetry (DSC) techniques. The FTIR measurements were made using a JASCO FT/IR-6300 (Jasco, Japan), with the KBr pelleting method, a resolution of 1 cm^{-1} , and a spectral range of 4000–400 cm^{-1} . The XRD was conducted in the 2θ range of 10–50 $^{\circ}$, using D8 Advance (Bruker, USA), with Cu K α radiation (45 kV, 36 mA) and a scan speed of 2 $^{\circ}/\text{min}$. The DSC was performed by DSC-1 STAR (Mettler Toledo, USA), with a scanning rate of 10 K/min, in the range of 50–250 $^{\circ}\text{C}$ under a nitrogen flow rate of 100 mL/min.

The crystallinity index (CI) was used to determine particle crystallinity, which is defined as the ratio of the material's crystalline proportion to the sum of its crystalline and amorphous fractions. The CI value was calculated using the FTIR signal intensities for the fibroin amide I and amide II bands^{9,42} (eqs 2 and 3). The signal intensities of the fibroin crystalline sections at amides I and II are D_{1622} and D_{1517} , respectively, while the signal intensities of the fibroin amorphous portions at amides I and II are D_{1646} and D_{1560} .

$$CI_{\text{IRI}} = \frac{D_{1622}}{D_{1622} + D_{1646}} \quad (2)$$

$$CI_{\text{IRI}} = \frac{D_{1517}}{D_{1517} + D_{1560}} \quad (3)$$

In Vitro CTX Release. The CTX release profile from the SFPs-CTX and PEG/SFPs-CTX was carried out by modeling the pH change of the gastrointestinal system.^{43,44} First, at 37 $^{\circ}\text{C}$ and constant shaking, the particles were dispersed in 10 mL of HCl pH 1.2, simulating the pH environment of the stomach, and CTX was released in 2 h. Then, the particles were

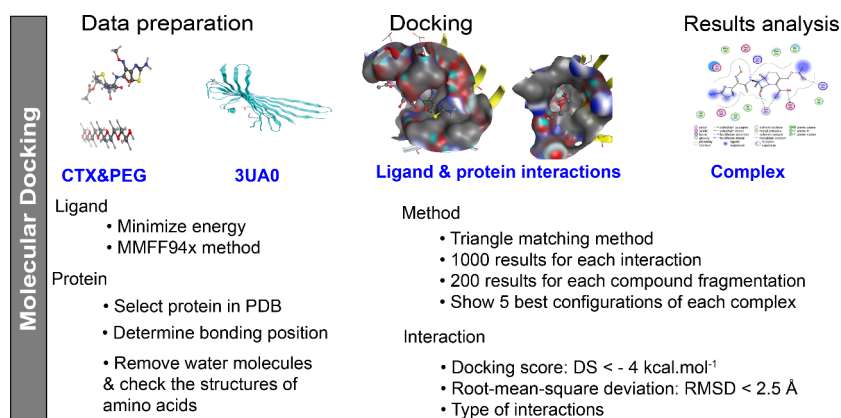


Figure 1. Procedure and molecular docking analysis of CTX, fibroin (3UA0), and PEG.

transferred into 30 mL of PBS buffer (pH 6.8), simulating the pH environment of the small intestine, and CTX was released in 4 more hours. At each 30 min survey time, exactly 2 mL of the sample was withdrawn and supplemented with 2 mL of the corresponding medium solution. The aspirates were centrifuged (18,000 rpm, 5 min), and the released CTX in the supernatant was quantified using UV-vis spectroscopy and the respective standard curves (concentration range of 0–10 $\mu\text{g/mL}$). For the HCl medium, the maximum absorption wavelength was 236 nm, and the regression equation was $y = 0.0258x + 0.0007$, $R^2 = 0.9986$; for the PBS medium, the wavelength was 204 nm, and the regression equation was $y = 0.037x - 0.0256$, $R^2 = 0.9966$. The cumulative CTX release percentage was calculated using eq 4. The release kinetics was also fitted with various models as described in Table 1.⁴⁵

$$\% \text{ cumulative CTX release} = \frac{C_t V_0 + V \sum_{i=1}^{t-1} C_i}{M_0 - \sum_{i=1}^{t-1} M_i} \times 100(\%) \quad (4)$$

where C_t and C_i are the concentrations of CTX released at time points t and i , V_0 is the entire volume of the buffer, V is the withdrawal sample volume at each time point (2 mL), M_0 is the initial quantity of CTX, and M_i is the total amount of CTX withdrawn at time point i .

2.6. Docking Analysis. To deeply understand the interactions among CTX, fibroin (3UA0 protein), and PEG in the particles, *in silico* docking was performed (Figure 1). Binding positions and interaction types, such as hydrogen bonds, van der Waals forces, and π – π interactions, were analyzed to evaluate the complex's affinity and stability.³⁷ The docking process was composed of two main steps.⁴⁶ First, the 3D structures of CTX and PEG were optimized to reach their minimum energy state. The MMFF94x force field was commonly used for small molecule geometry optimization, ensuring correct bond lengths, angles, and torsion energies, which helps stabilizing the ligand conformation. The 3UA0 protein was retrieved from the Protein Data Bank (PDB), which provides experimentally determined protein structures, and the water molecules were removed to avoid unwanted artifacts. Second, the docking phase involved computational techniques to simulate and evaluate the ligand's binding to the protein, utilizing the triangle matching method, with 1000 docking and 200 fragmentation configurations. Each docked pose was evaluated using a scoring function, which measures binding affinity by considering hydrogen bonds, van der Waals

forces, and π – π interactions. The docking score (DS) reflects the predicted free energy of binding (i.e., < -4 kcal/mol is considered strong binding). Configurations with the lowest docking scores (best binding energies) and acceptable conformational root-mean-square deviation ($\text{RMSD} < 2.5 \text{ \AA}$) were selected for further analysis.

2.7. Molecular Dynamics Simulation. MD simulations were conducted following three main steps, as follows: (1) Data preparation: Ligands and proteins were optimized by adding hydrogen atoms, applying the CHARMM-27 force field, and generating topology before forming the ligand–protein complex.³⁸ (2) MD simulation: The system was placed in a solvated dodecahedron box (1.0 nm from boundaries), neutralized with ions (0.15 M NaCl), energy minimized, and equilibrated at 300 K and 1 bar before MD simulation. (3) Result analysis: The stability of the complex was assessed by using RMSD and root-mean-square fluctuation (RMSF), and interaction types were analyzed to understand system dynamics and stability.

2.8. Greenness Assessment of Process. To assess the greenness and the environmental effect of SFPs formulation processes (i.e., co-condensation and adsorption), this study employed the Ecochain Mobious software for LCA of experimental techniques, with standard 25 output variables. Ecochain Technologies, located in The Netherlands, created this software, which has been certified 9001:2015 and 27001:2017 by the International Organization for Standardization (ISO).⁴⁷ The input factors analyzed and employed in the assessment included electrical energy, solvents, and chemicals. Ecoinvent v3.9.1 was incorporated into the Ecochain Mobious software as a database for the LCA study, which complied with international standards like ISO 14040 and ISO 14044.⁴⁸

2.9. Statistical Analysis. The quantitative experiments were carried out a minimum of three times and presented as mean \pm standard deviations (SDs). Statistical comparisons were conducted using the Student's t test and one-way analysis of variance (Excel) with a significant p -value of < 0.05 .

3. RESULTS AND DISCUSSION

3.1. Particle Physicochemical Properties. Size, Size Distribution, EE%, Charge, and Morphology. First, by variation of the fibroin concentration (SFPs-0.5 and SFPs-1), the particle size significantly increased from 378 nm (492 nm for CTX-loaded particles) with a fibroin concentration of 0.5% to 451 nm (633 nm for CTX-loaded particles) with a fibroin

Table 2. Particle Size, Size Distribution (Polydispersity Index, PI), Charge, and Entrapment Efficiency (EE%) of SFPs and PEG/SFPs ($n = 3$)^a

	particles	SFPs-0.5	SFPs-1	PEG/SFPs-0.5	PEG/SFPs-1
size (nm)	blank	378.4 ± 11.1 ^a	451.4 ± 20.5 ^{bc}	194.0 ± 8.1 ^e	165.8 ± 11.9 ^g
	CTX-loaded (co-condensation)	492.0 ± 16.2 ^b	633.1 ± 15.0 ^d	247.8 ± 10.7 ^f	212.2 ± 12.1 ^h
	CTX-loaded (adsorption)	389.2 ± 10.3 ^a	446.6 ± 19.2 ^{bc}	195.1 ± 10.4 ^e	171.9 ± 13.0 ^g
PI	blank	0.214 ± 0.013	0.182 ± 0.012	0.208 ± 0.031	0.176 ± 0.018
	CTX-loaded (co-condensation)	0.179 ± 0.021	0.151 ± 0.019	0.194 ± 0.017	0.189 ± 0.022
	CTX-loaded (adsorption)	0.144 ± 0.015	0.162 ± 0.010	0.185 ± 0.026	0.173 ± 0.011
charge (mV)	blank	−31.1 ± 1.4 ^a	−30.5 ± 1.8 ^a	−25.3 ± 1.1 ^b	−23.2 ± 1.3 ^b
	CTX-loaded (co-condensation)	−32.2 ± 2.5 ^a	−30.7 ± 1.7 ^a	−24.6 ± 1.0 ^b	−22.8 ± 1.1 ^b
	CTX-loaded (adsorption)	−30.1 ± 1.5 ^a	−31.1 ± 1.0 ^a	−23.9 ± 2.0 ^b	−25.0 ± 1.6 ^b
CTX EE%	co-condensation	55.7 ± 4.1 ^a	56.2 ± 3.7 ^a	55.9 ± 4.3 ^a	57.2 ± 4.2 ^a
	adsorption	52.6 ± 3.8 ^a	54.1 ± 3.9 ^a	57.8 ± 4.0 ^a	57.7 ± 4.0 ^a

^aDifferent letters (a–h) denote significant differences between samples in the same category.

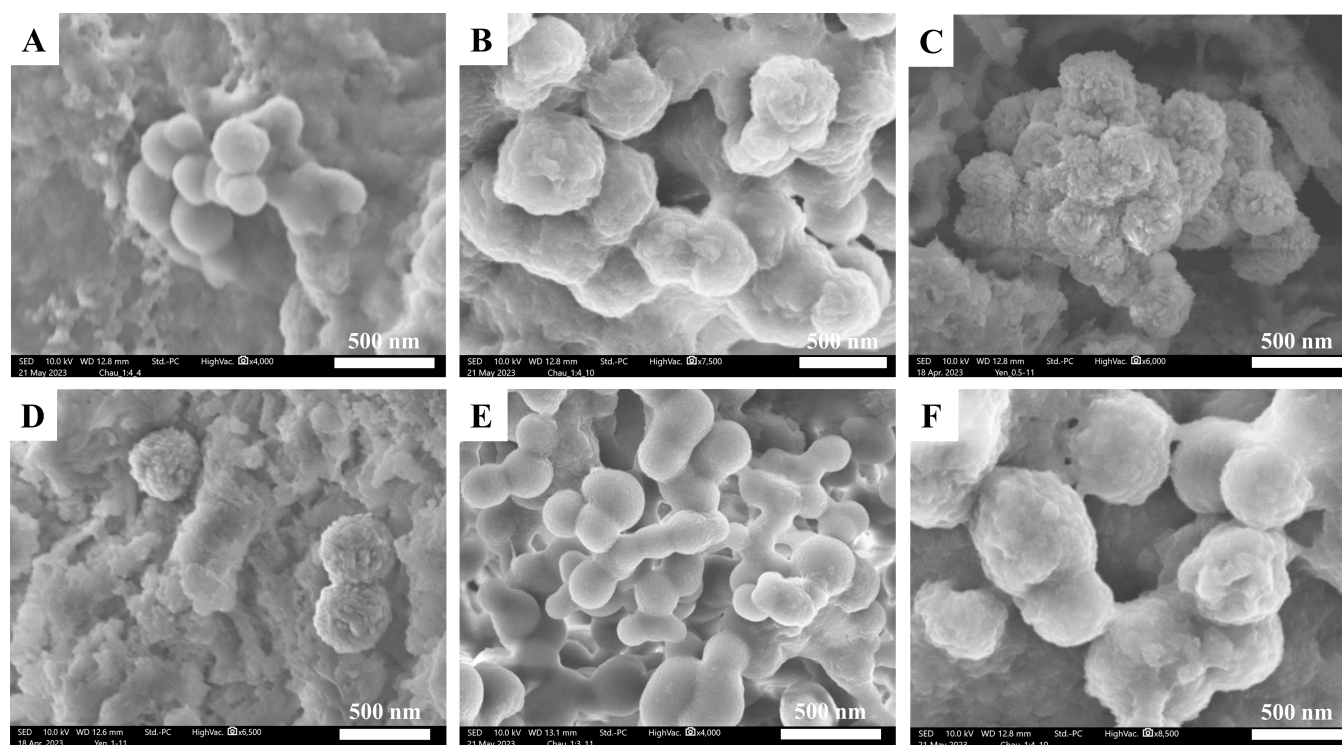


Figure 2. SEM images of (A) SFPs, (B) PEG/SFPs, (C) SFPs-CTX formulated by the co-condensation method, (D) PEG/SFPs-CTX formulated by the co-condensation method, (E) SFPs-CTX formulated by the adsorption method, and (F) PEG/SFPs-CTX formulated by the adsorption method.

concentration of 1% (Table 2). This phenomenon occurred due to the aggregations of fibroin molecules during the condensation process. Consequently, as the fibroin concentration increased, the number of fibroin molecules presented in the solution also rose, promoting aggregation and resulting in the formation of larger particles.^{10,49} Expectedly, these aggregations were reduced with the incorporation of PEG, yielding smaller particles.¹⁹ The higher the PEG concentration is, the smaller are the particle sizes. PEG reduces SFP aggregation primarily due to the steric stabilization effect. PEG chains form a dense, brush-like layer on the SFP surface, thus preventing SFPs from coming close enough to aggregate. When two PEG/SFPs approach each other, the PEG chains compress, which are energetically unfavorable. This steric repulsion kept the particles apart.

Second, the incorporation of CTX significantly increased the particle size in the co-condensation method but not in the adsorption method (Table 2). This was due to the fact that in the co-condensation method, the drug molecules condensed (i.e., precipitated) from the aqueous phase simultaneously with the fibroin molecules. Therefore, CTX was mostly encapsulated in the particle core (i.e., matrix type), thus enlarging the particle sizes. On the other hand, in the adsorption method, CTX was in the molecular dispersion form and only adhered on the particle surfaces during the formulation process. Consequently, the particles sizes did not alter much compared to the blank counterparts. Regarding the size distribution, all formulas possessed narrow size distribution patterns, with PI of <0.3.⁵⁰

For the particle charges, the nonfunctionalized SFPs showed a negative surface charge, corresponding to the inherent fibroin

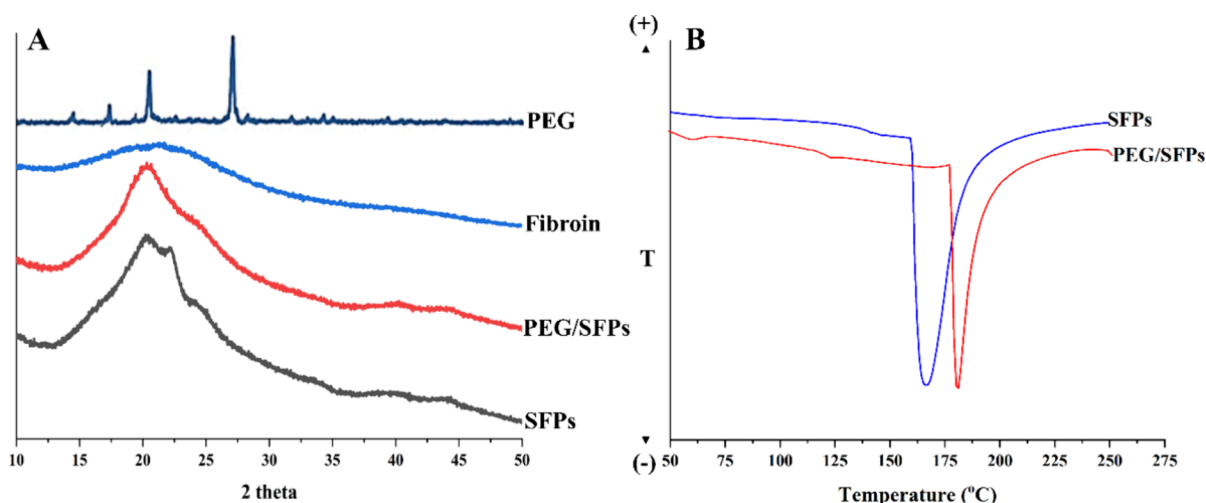


Figure 3. (A) XRD pattern and (B) DSC spectra of the particles. For comparison purposes, the graphs were regenerated from the numerical data obtained during the experiments using the Origin software.

negative zeta potential at pH 7.0.⁵¹ The functionalization with PEG slightly reduced the particle surface charge, possibly due to the coating effect of PEG. Since PEG is coated on the particle surfaces and it is a noncharged moiety at pH 7.0, the overall zeta potentials of the systems were decreased. Another issue to notice was that the CTX incorporation did not alter the particle charge, which was because CTX is nonionized at pH 7.0.

In terms of the CTX EE%, both formulation methods and both particle types (i.e., nonfunctionalized and PEG-functionalized) yielded similar EE% of ~ 50%, demonstrating that the loading capacity of the particle system remains constant when PEG is included in the particle structure. The EE% of 50%, although not high, is generally considered adequate for the nanoparticulate system in encapsulating and delivering pharmaceutical compounds.^{13,49}

Lastly, under SEM imaging (Figure 2), the particles appeared to be spherical. Interestingly, compared to the blank SFPs, which possessed a smooth morphology and an aggregated pattern (in agreement with previous studies^{14,15}), the PEG/SFPs showed more uniform unaggregated particles with a rougher surface. This was due to the coating effect and steric hindrance effect of PEG, as previously discussed. Regarding the formulation methods, CTX-loaded particles formulated by the co-condensation method demonstrated clear CTX crystalline crystals on the particle surfaces due to the fact that CTX was co-condensed (i.e., coprecipitated) with fibroin molecules, changing its polymorph from amorphous in the aqueous solution to crystalline in the particles.⁴⁴ On the other hand, CTX-loaded particles formulated by the adsorption method showed no observable crystals, indicating that the CTX was adsorbed onto the particle surfaces as a molecular amorphous form.

Conclusively, the two distinct formulation methods resulted in particles with similar PI, charge, and EE% but different sizes (co-condensation > adsorption) and morphology (rough with surface CTX crystal in co-condensation and smooth with surface CTX molecules in adsorption). These differences significantly affected the particle release properties, as discussed later.

Chemical Interactions and Crystallinity. The XRD pattern (Figure 3A) reveals the typical fibroin structure, which has a

large peak at around $2\theta = 20^\circ$. The SFPs sample has a similar structure to that of the fibroin powder, but the intensity of the peak rises due to fibroin's structural change from amorphous α -helices to antiparallel β -sheet in the particles, which enhances crystallinity.⁹ The PEG/SFP sample has a similar structure to SFPs and lacks the typical PEG peaks because the PEG concentration in the sample was low (i.e., 0.5 and 1%). This means that the PEG functionalization did not significantly alter the fibroin structure. Furthermore, the DSC spectra (Figure 3B) of SFP and PEG/SFPs particles differ in the phase transition temperatures, which are 140 and 125 °C, respectively. This suggests that the incorporation of PEG, an amorphous polymer, slightly reduces the thermal stability of the whole system.

The interaction of the components in the particulate system with CTX is shown through the FTIR spectrum (Figure 4). To

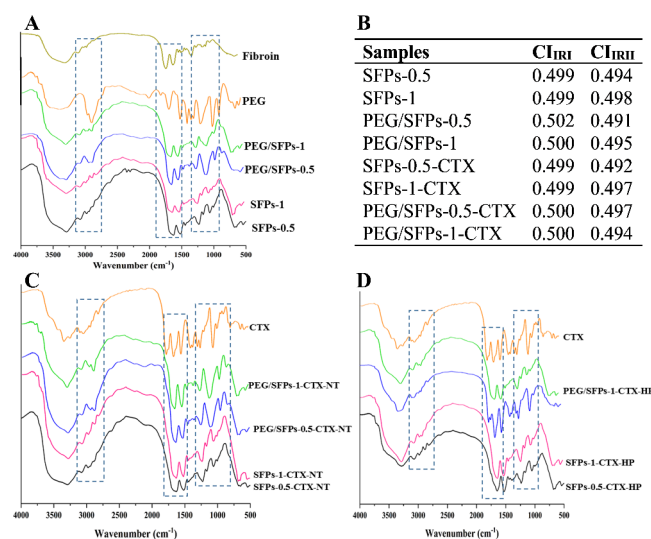


Figure 4. (A) FTIR spectra of the blank particles, (B) crystallinity (CI), (C) FTIR spectra of CTX loaded particles by the co-condensation method, and (D) FTIR spectra of CTX loaded particles by the adsorption method. For comparison purposes, the graphs were regenerated from the numerical data obtained during the experiments using the Origin software.

this end, the FTIR spectra of the blank particles demonstrated the distinctive structure of fibroin at 1626–1620 cm^{-1} (amide I, C=O stretching vibration), at 1515–1526 cm^{-1} (amide II, N–H bending vibration), and at 1231–1261 cm^{-1} (amide III, C–N and N–H functional groups).^{15,42} The PEG/SFPs particles exhibited the typical PEG peak at 2878 cm^{-1} , which represents the vibration of the methylene group in the PEG structure.⁵² As a result, the FTIR spectrum confirmed that PEG was effectively incorporated into the SFPs. In terms of the CTX-loaded particles, the FTIR spectra showed recognizable CTX peaks in particles formulated by both co-condensation and adsorption techniques. CTX's structure includes the C–O functional group of the β -lactam ring, which corresponds to position 1759 cm^{-1} .⁵³ The distinctive peaks of CTX coincide with the signals of fibroin and PEG in the condensation technique; therefore, the FTIR spectrum does not clearly show the peak location. On the other hand, the drug molecules adsorbed on the particle surface in the adsorption approach, allowing the distinctive peaks of CTX to be identified when evaluating the FTIR spectra. Furthermore, the CI values of the particles before and after drug loading remained constant, indicating that CTX had no effect on the particle structure.

Adsorption Study. To further understand the mechanisms of CTX adsorption into the particles in the adsorption preparation method, an in-depth analysis was conducted. For this, the SFPs and PEG/SFPs exhibit comparable CTX adsorption capabilities under the same circumstances (Figure 5). The adsorption process was quick and efficient for the first

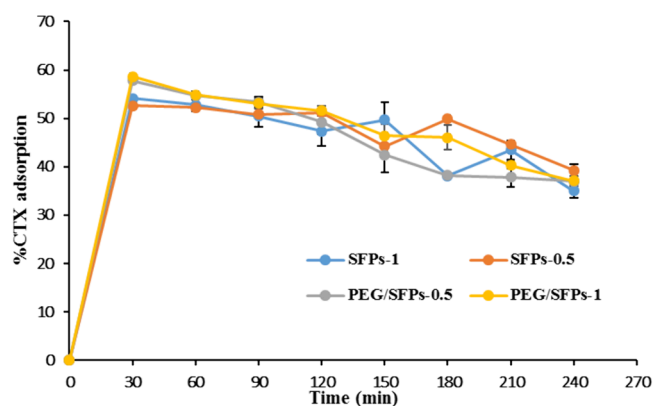


Figure 5. Adsorption process of CTX over time of the particles ($n = 3$).

30 min, reaching $\sim 50\%$, after which it progressively diminished. Because CTX is a big molecule, the interactions between the particle and drug molecules consists mostly of weak hydrogen bonds, van der Waals forces, and π – π interactions (further discussed in the docking section). Thus, if the drug molecules occupy the adsorption sites, the adsorption process is nearly balanced. As a result, after 30 min, the adsorption effectiveness decreased due to the desorption of CTX from the particles into the surrounding environment. The D–R model demonstrates that CTX adsorption processes were completely physical, with $E < 8$ kJ/mol (Table 3). The adsorption kinetics equation demonstrates that the adsorption process followed second-order adsorption kinetics (Table 3). The small slope coefficient suggests that the adsorption process was rapid, which was entirely consistent with the experimental results.

In Vitro CTX Release. The CTX release investigation from the particle system was carried out by imitating the pH change of the digestive tract. For the first 2 h, the release medium was simulated gastric juice (HCl pH 1.2) followed by 4 h of simulated small intestine juice (PBS buffer pH 6.8). The release process differs significantly from the particles formulated by the co-condensation and adsorption methods (Figure 6). In a pH 1.2 setting, the co-condensation approach has a poor drug release efficiency, i.e., around 10% in 2 h. This was due to the limited solubility of CTX crystals, which are located on the particle surfaces, at pH 1.2. CTX has a pK_a of 2.73; thus, at pH 1.2, CTX solubility significantly decreases due to the protonation of functional groups. When the environment changed, the release efficiency of all four types of particles improved linearly at pH 6.8. This was again due to the solubility of CTX; at neutral pH, the CTX solubility is generally good, making it suitable for formulation in injectable forms. The neutral pH is optimal for cefotaxime's stability as well. Accordingly, PEG/SFPs-1-CTX particles had the highest release efficiency ($52.88 \pm 0.9\%$) followed by PEG/SFPs-0.5-CTX, SFPs-1-CTX, and SFPs-0.5-CTX. The PEG/SFPs had a higher release ability than the SFPs because PEG serves as a surfactant, emulsifying the CTX and boosting both release time and percentage. Moreover, PEG is a water-soluble polymer; thus, coating the particles with PEG improves wettability and solubility,⁵⁴ resulting in high release efficiency. Additionally, the PEG/SFPs had smaller particle sizes than those of SFPs, consequently increasing the surface-area-to-volume ratio and enhancing the particle contact with the surrounding medium.

Table 3. Parameters of First-Order Kinetics, Second-Order Kinetics, and the D–R Model for the CTX Adsorption Process

model	sample	R^2	q_e (mg/g)	K_1	K_2	E (kJ/mol)
first-order kinetics	SFPs-0.5	0.1530	1.84	−0.0023		
	SFPs-1	0.0587	1.30	0.0015		
	PEG/SFPs-0.5	0.5024	6.57	0.0119		
	PEG/SFPs-1	0.0572	3.39	0.0035		
second-order kinetics	SFPs-0.5	0.9934	18.72		0.0029	
	SFPs-1	0.9825	17.57		0.0032	
	PEG/SFPs-0.5	0.9845	17.27		0.0034	
	PEG/SFPs-1	0.9958	17.79		0.0032	
D–R	SFPs-0.5	0.9928				0.42
	SFPs-1	0.9765				0.41
	PEG/SFPs-0.5	0.9916				0.38
	PEG/SFPs-1	0.9980				0.42

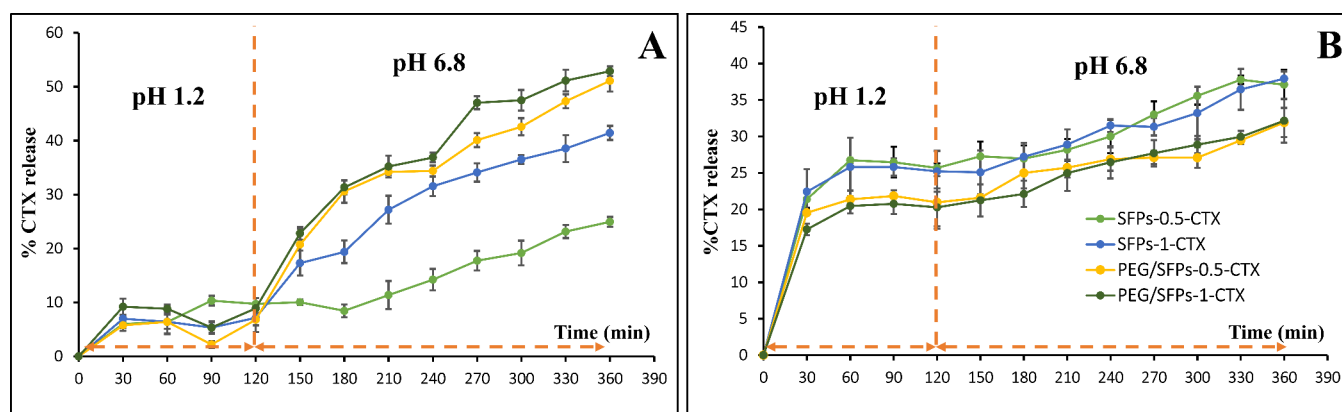


Figure 6. Release profile of CTX loaded particles formulated by the (A) co-condensation method and (B) adsorption method.

Table 4. Parameter Values of the Release Kinetic Models of Nanoparticles Formulated by the Co-condensation and Adsorption Method

method	model	SFPs-0.5	SFPs-1	PEG/SFPs-0.5	PEG/SFPs-1
co-condensation	zero-order	$R^2 = 0.8455, k_0 = 0.0972$	$R^2 = 0.8825, k_0 = 0.1504$	$R^2 = 0.8553, k_0 = 0.1745$	$R^2 = 0.8554, k_0 = 0.1892$
	first-order	$R^2 = 0.8417, k_1 = 0.0005$	$R^2 = 0.9281, k_1 = 0.0009$	$R^2 = 0.9707, k_1 = 0.0009$	$R^2 = 0.9225, k_1 = 0.0012$
	Higuchi	$R^2 = 0.8647, k_H = 2.3844$	$R^2 = 0.9901, k_H = 2.6591$	$R^2 = 0.9811, k_H = 3.1195$	$R^2 = 0.9832, k_H = 3.3873$
	Hixson–Crowell	$R^2 = 0.8431, k_{HC} = -0.0017$	$R^2 = 0.9142, k_{HC} = -0.0028$	$R^2 = 0.9011, k_{HC} = -0.0034$	$R^2 = 0.9028, k_{HC} = -0.0038$
	Peppas	$R^2 = 0.9585, n = 0.5778$	$R^2 = 0.9786, n = 0.6764$	$R^2 = 0.9668, n = 0.7069$	$R^2 = 0.9670, n = 0.7215$
adsorption	zero-order	$R^2 = 0.7460, k_0 = 0.0889$	$R^2 = 0.7864, k_0 = 0.0890$	$R^2 = 0.8307, k_0 = 0.1094$	$R^2 = 0.8533, k_0 = 0.1211$
	first-order	$R^2 = 0.7876, k_1 = 0.0005$	$R^2 = 0.8263, k_1 = 0.0003$	$R^2 = 0.8750, k_1 = 0.0006$	$R^2 = 0.8990, k_1 = 0.0007$
	Higuchi	$R^2 = 0.9287, k_H = 1.6560$	$R^2 = 0.9493, k_H = 1.6350$	$R^2 = 0.9700, k_H = 1.9737$	$R^2 = 0.9820, k_H = 2.1696$
	Hixson–Crowell	$R^2 = 0.7740, k_{HC} = -0.0016$	$R^2 = 0.8134, k_{HC} = -0.0016$	$R^2 = 0.8610, k_{HC} = 0.0020$	$R^2 = 0.8846, k_{HC} = 0.0022$
	Peppas	$R^2 = 0.9436, n = 0.5961$	$R^2 = 0.9542, n = 0.5918$	$R^2 = 0.9613, n = 0.6236$	$R^2 = 0.9668, n = 0.6397$

Table 5. Energy, Distances, and Types of Interactions among CTX, Fibroin (3UA0), and PEG^a

ligands	DS	RMSD (Å)	E_conf	E_place	E_score1	E_refine	E_score2
CTX	−6.018	0.716	3.531	−84.887	−10.657	−31.809	−6.018
PEG	−5.935	1.391	2.049	−66.805	−10.645	−32.635	−5.935
CTX		interactions			distance (Å)		E (kcal/mol)
O	45	OE1	GLU 94 (A)	H-donor	2.96		−4.3
O	17	NZ	LYS 82 (B)	H-acceptor	3.54		−2.3
O	21	NE2	GLN 65 (B)	H-acceptor	2.94		−0.8
O	47	NE2	GLN 65 (B)	H-acceptor	2.95		−1
PEG		interactions			distance (Å)		E (kcal/mol)
OH3	1	OE1	GLU 94 (B)	H-donor	2.83		−2.4
OH4	9	CA	ASN 24 (B)	H-acceptor	3.44		−0.7
OH7	30	N	ILE 23 (B)	H-acceptor	3.32		−3.2

^aDistance: RMSD (Å).

For the adsorption approach, all four particle systems rapidly release CTX in the HCl environment because the drug was loaded via adsorption on the particle surface. Thus, the drugs were in the amorphous forms; hence, when in contact with the buffer, CTX was quicker to release than the drug condensed in the particles. Moreover, no significant difference was observed between the drug release effectiveness of the four types of particles formulated by the adsorption method.

The kinetic calculations suggest that the release mechanism followed the Higuchi and Korsmeyer–Peppas models (Table 4). According to the Higuchi model, the drug's solubility determines the release mechanism; water-soluble medicines have a favorable release profile.^{55,56} This is consistent with CTX high solubility in PBS at pH 6.8. Moreover, the drug release process aligns with the Korsmeyer–Peppas model's

diffusion–disintegration mechanism since all SFPs-0.5, SFPs-1, PEG/SFPs-0.5, and PEG/SFPs-1 particles have n values between 0.45 and 0.9.⁵⁷ Furthermore, depending on the particle structure, the polymer chain created has a matrix structure with holes that aid in drug diffusion. The structure of PEG/SFP particles comprises PEG, a water-soluble polymer, which can erode and destroy the particle structure during the release process. As a result, both particles formed by the co-condensation and adsorption methods had identical release processes in the small intestine environment.

Last but not least, it is worth noting that not 100% of CTX was released into the medium, which could be due to the fact that some CTX may remain within the SFPs due to strong interactions with fibroin (proven by the *in silico* docking results). Thus, it is likely that the remaining CTX will continue

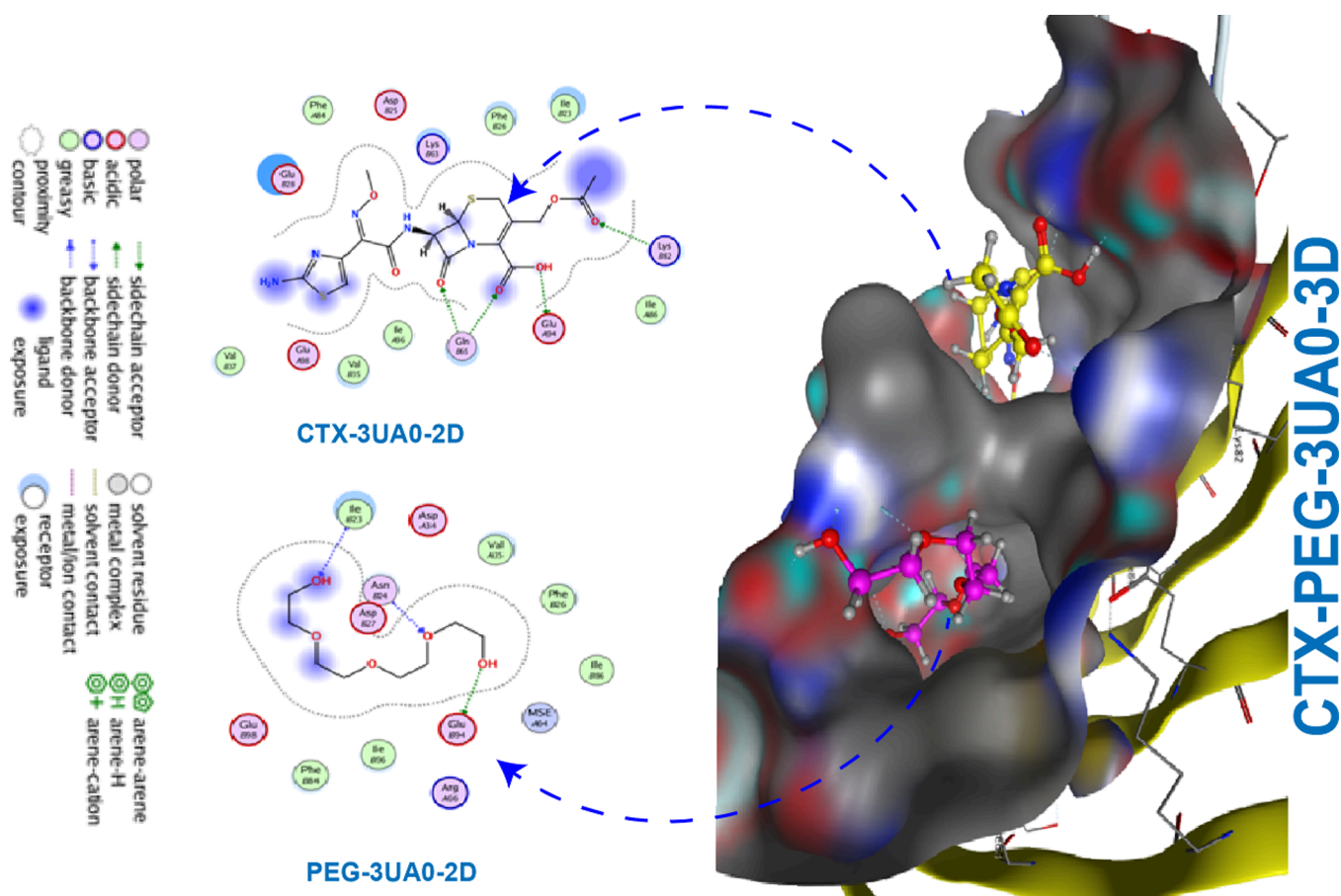


Figure 7. Two- and three-dimensional molecular interaction analyses of CTX, fibroin (3UA0), and PEG.

to be released over an extended period. However, because the common gastrointestinal retention time is 6 h, we did not prolong the study release time. Future studies with a prolonged release time could be conducted to confirm this hypothesis.

3.2. Docking Analysis and MD Simulation. *Docking Analysis.* To further investigate the interactions between CTX, fibroin, and PEG in the particles, *in silico* docking study and MD simulation were employed. First, the docking results show that both CTX and PEG demonstrate stable binding, as indicated by their low DS values (−6.018 and −5.935, respectively) (Table 5 and Figure 7). RMSD values indicate slightly higher deviation for PEG compared to CTX. CTX shows slightly better refinement and final score (E_{score2}) compared to PEG, suggesting slightly more favorable binding. When CTX and PEG are simultaneously present, the binding site changes and the bond strength increases, as evidenced by the shortening of the hydrogen bond lengths.

Specifically, CTX forms strong H-donor and H-acceptor bonds with the most significant interaction (−4.3 kcal/mol) involving OE1 of GLU 94. The hydrogen bond distances were within the ideal range (2.5–3.5 Å), ensuring interaction stability. CTX achieved a DS of −6.018, indicating strong ligand–protein affinity, with an RMSD value of 0.716 Å, demonstrating stability postoptimization. DS values below −5 are generally considered good, with lower values indicating more stable binding. The E_{conf} of 3.531 states that CTX exhibits a relatively higher conformational energy, indicating that it undergoes significant structural adjustments upon binding to fit the fibroin pocket. The highly negative

E_{place} value (−84.887) reflects the strong initial placement of CTX in the binding pocket driven by its compatibility with the fibroin active site. The E_{refine} of −31.809 suggests that the interactions were mainly noncovalent forces such as hydrogen bonds, van der Waals forces, and π – π interactions.

For PEG, PEG forms weaker bonds compared to CTX, with the strongest interaction (−3.2 kcal/mol) involving the N of ILE 23. The DS for PEG was −5.935, reflecting significant ligand–protein affinity, with an RMSD value of 1.391 Å, ensuring structural stability. This is consistent with its smaller size and simpler structure, leading to fewer opportunities for specific interactions. A small E_{conf} of 2.049 indicates that PEG requires less conformational adjustment than CTX, likely due to its flexible and less complex structure. The van der Waals forces and π – π interactions between PEG and fibroin aromatic residues (i.e., Phe826) further enhanced the complex's stability.

In combination, CTX and PEG can exert a strong binding tendency with GLU during protein binding due to the hydroxyl and carbonyl functional groups in their structures. The π – π interactions play an important role in stabilizing the binding, reducing the system energy, and explaining the high affinity of both of these substances for fibroin. Overall, PEG was found to not cause any loss of stability or hinder the interaction between CTX and fibroin, ensuring that the combined system PEG/SFPs-CTX is highly stable and compatible in the digestive environment. In particular, fibroin and PEG have the ability to protect CTX, a sensitive antibiotic that is easily degraded by digestive enzymes (such as β -lactamase and, protease) and

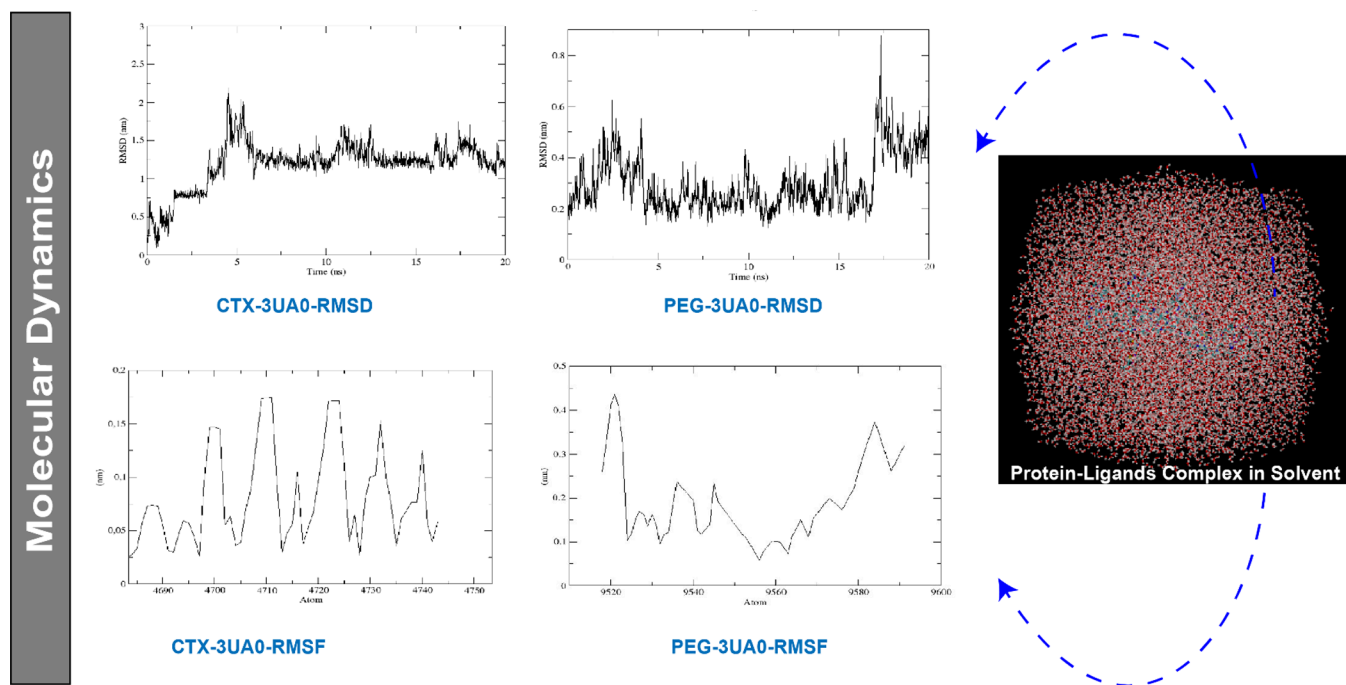


Figure 8. Molecular dynamics analysis of CTX–PEG–fibroin (3UA0) complexes.

gastric acid pH, by forming strong bonds, helping to enhance the protective and stable effect of CTX in the drug delivery system.

MD Simulation. MD simulation in a physiological aqueous environment (pH 6.8) confirmed the system's physiological relevance (Figure 8). For this, the PEG/SFPs-CTX was surrounded by an ion-neutralized aqueous solvent environment, demonstrating that the simulation was performed under physiological conditions. This ensured that the complex was tested in an environment similar to real-life conditions, helping to assess the biocompatibility of the system. The CTX–fibroin complex showed RMSD values of 1.0–2.0 nm after 5 ns, indicating adequate stability in the buffer. The PEG–fibroin interactions displayed lower RMSD values (0.4–0.6 nm), suggesting minimal structural disturbance by PEG in the PEG/SFPs-CTX particles. RMSF analysis showed stable protein regions (<0.2 nm) and confirmed that PEG's interaction did not destabilize the fibroin structure. Furthermore, the RMSF results show the degree of fluctuation of specific regions in the fibroin protein when bound to CTX and PEG. With CTX, the RMSF is concentrated in the side chains, while the core structure has low values (<0.2 nm), indicating the stability of the complex. For PEG, the RMSF of the polymer-exposed regions fluctuates below 0.4 nm, ensuring that PEG does not destabilize or disrupt the protein structure.

In conclusion, the MD simulation reveals that, in the physiological environment, both CTX and PEG interactions with fibroin are stable, with RMSD profiles confirming this over time. The CTX–fibroin composite reached equilibrium after 5 ns with good RMSD and RMSF, ensuring effective binding. Moreover, PEG conjugation potentially enhances the structural rigidity in some regions, as observed in RMSF profiles. The solvated models ensure a realistic interaction behavior, which is critical for understanding the complex's dynamics. This result confirms the ability of the PEG/SFPs-CTX to protect CTX and supports its application as an effective drug delivery system.⁵⁸

3.3. Greenness Assessment of the Process. In recent years, “sustainable chemistry” has gained increased attention from scientists and environmental activists, and the trend of “green” and “environmental friendly” has grown popular. As a result, rather than focusing on the finished product, emphasis has been directed toward the potential negative environmental implications of the entire production cycle, including raw materials, manufacture, use, and reuse. To regulate variables that might have an adverse effect on the environment and minimize needless inputs, the solvents, chemicals, and energy used in the production of nanoparticles should be carefully selected, controlled, and optimized. For this, several studies have chosen to employ LCA to evaluate the life cycle of nanoparticle formulation processes.^{59–62}

However, there has been no study applying the LCA assessment to evaluate the formulation process greenness of the PEG/SFPs-CTX. As a result, LCA was applied for the first time throughout this procedure. To ensure the use of ecologically safe solvents, both formulation methods predominantly rely on aqueous solvents of water and ethanol, which inherently reduce environmental and health risks. Ethanol was used as a precipitating agent in the co-condensation method, which is considered a relatively green solvent due to its low toxicity and biodegradability. Ethanol is classified as a Class 3 solvent according to ICH guidelines, indicating a low risk to human health and the environment (Figure 9). Regarding chemicals and waste, fibroin and PEG, the main biomaterials used, are biocompatible and biodegradable. In addition, the research prioritized the use of locally accessible raw materials, such as silkworm cocoons, to reduce emissions from transportation vehicles. The process of CTX loading is achieved through either direct co-condensation or adsorption. Neither method requires hazardous cross-linkers or stabilizers, reducing the risk of toxic waste generation. Additionally, the washing steps in both methods involve only distilled water, reducing chemical waste and hazardous effluent production. In terms of the energy consumption, both methods employed

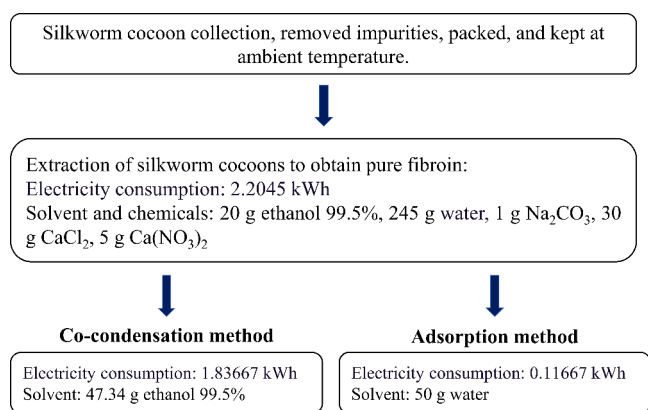


Figure 9. Schematic flowchart of the PEG/SFPs-CTX formulation process using two distinct approaches of co-condensation and adsorption.

simple techniques of stirring, centrifugation, and drying, which minimize the power usages.

The LCA results illustrate the potential effects of the co-condensation method (1) and adsorption method (2) on the environment (Table 6). These effects fall under several impact groups, including eutrophication (EU), ozone depletion (OD), human toxicity (HT), ecotoxicity (EC), climate change (CC),

and acidification (AC). Specially, CC, AC, EC, and HT are some of the primary effect categories that are frequently taken into account while evaluating LCA because these outputs have the ability to seriously affect the environment, destroy the natural ecological balance, and create risks that might endanger both animal and human life.⁵⁹

In general, both formulation processes of co-condensation and adsorption do not have much impact on the environment. First, regarding AC, taking ocean acidification as an example, atmospheric CO₂ when dissolved in water will create H₂CO₃, which after dissociation will release H⁺ ions. This will cause the pH to decrease (from about 8.2 to lower), seriously threatening marine life, especially species that depend on calcium carbonate.⁶³ Similar to the soil environment, the acid deposition process from rain containing H₂SO₄ or HNO₃ will also produce ions through chemical reactions, causing the soil to lose its nutritional balance and releasing heavy metals such as Al³⁺, which lead to negative consequences such as soil degradation, causing harm to crops.⁶⁴ For these reasons, it is necessary to consider the possible AC level of experimental processes to control CO₂, SO₂, and NO_x emissions to minimize AC. Both PEG/SFPs-CTX processes showed AC of 3.27·10⁻³ and 6.38·10⁻³ mol H⁺ equiv, respectively, which are equivalent to 1.02·10⁻⁴ and 1.99·10⁻⁴ kg SO₂ equiv. These values are significantly lower than the allowable AC values

Table 6. Greenness Assessment Parameters (Input, Output) of the Two Employed Nanoparticles Formulation Processes of (Method 1) Co-condensation and (Method 2) Adsorption

input			
co-condensation method (1)		adsorption method (2)	
solvents and chemicals	67.34 g ethanol 99.5%, 245 g water, 5 g Ca(NO ₃) ₂ , 1 g Na ₂ CO ₃ , and 30 g CaCl ₂	20 g ethanol 99.5%, 295 g water, 5 g Ca(NO ₃) ₂ , 1 g Na ₂ CO ₃ , and 30 g CaCl ₂	
electricity consumption	0.7 kWh (electric stove), 0.037 kWh (microwave), 1.44 kWh (magnetic stirrer), 0.06417 kWh (centrifuge), and 1.8 kWh (refrigerator)	0.7 kWh (electric stove), 0.037 kWh (microwave), 1.52 kWh (magnetic stirrer), and 0.06417 kWh (centrifuge)	
output			
impact category name	reference unit	method (1)	method (2)
acidification	mol H ⁺ equiv	6.38 × 10 ⁻³	3.27 × 10 ⁻³
climate change	kg CO ₂ equiv	8.39 × 10 ⁻¹	4.27 × 10 ⁻¹
climate change—biogenic	kg CO ₂ equiv	1.19 × 10 ⁻³	7.39 × 10 ⁻⁴
climate change—fossil	kg CO ₂ equiv	8.37 × 10 ⁻¹	4.26 × 10 ⁻¹
climate change—land use and LU change	kg CO ₂ equiv	6.81 × 10 ⁻⁴	3.30 × 10 ⁻⁴
ecotoxicity, freshwater	CTUe	1.20 × 10 ¹	5.68
ecotoxicity, freshwater—inorganics	CTUe	1.02 × 10 ¹	4.98
ecotoxicity, freshwater—organics	CTUe	1.79	6.97 × 10 ⁻¹
eutrophication, freshwater	kg P equiv	1.36 × 10 ⁻⁴	7.02 × 10 ⁻⁵
eutrophication, marine	kg N equiv	3.95 × 10 ⁻³	1.29 × 10 ⁻³
eutrophication, terrestrial	mol N equiv	1.16 × 10 ⁻²	5.11 × 10 ⁻³
human toxicity, cancer	CTUh	6.78 × 10 ⁻¹⁰	3.56 × 10 ⁻¹⁰
human toxicity, cancer—inorganics	CTUh	4.47 × 10 ⁻¹⁰	2.36 × 10 ⁻¹⁰
human toxicity, cancer—organics	CTUh	2.31 × 10 ⁻¹⁰	1.21 × 10 ⁻¹⁰
human toxicity, noncancer	CTUh	3.66 × 10 ⁻⁸	1.73 × 10 ⁻⁸
human toxicity, noncancer—inorganics	CTUh	3.54 × 10 ⁻⁸	1.67 × 10 ⁻⁸
human toxicity, noncancer—organics	CTUh	1.18 × 10 ⁻⁰⁹	5.98 × 10 ⁻¹⁰
ionizing radiation	kBq U235 equiv	1.13 × 10 ⁻²	5.42 × 10 ⁻³
land use	Pt	1.73 × 10 ¹	5.55
ozone depletion	kg CFC11 equiv	2.12 × 10 ⁻⁸	1.03 × 10 ⁻⁸
particulate matter	disease inc.	3.54 × 10 ⁻⁸	1.73 × 10 ⁻⁸
photochemical ozone formation	kg NMVOC equiv	2.51 × 10 ⁻³	1.22 × 10 ⁻³
resource use and fossils	MJ	1.05 × 10 ¹	5.37
resource use, minerals, and metals	kg Sb equiv	1.86 × 10 ⁻⁵	1.06 × 10 ⁻⁵
water use	m ³ -world equiv	1.14	1.40 × 10 ⁻¹

(ranging from 1.0 to 20.0 kg SO₂ equiv⁵⁹). Therefore, it can be concluded that the two processes are not potential threats that can cause AC.

CC is also a major concern, which quantifies and converts the impacts of greenhouse gases (CH₄ and N₂O) to a value deemed comparable to CO₂ based on the potential for global warming. Extreme weather, storms, floods, droughts, threats to biodiversity, air pollution, and a host of societal issues (resource disputes) are just a few of the major effects that CC may have on Earth. For the reasons listed above, lowering the quantity of CO₂ equiv emissions is a problem that requires attention to fight CC.⁶⁵ For the co-condensation process, the CC-inducing potential ranges from 6.81.10⁻⁴ to 0.839 kg CO₂ equiv, and for the adsorption method, this number ranges from 3.30.10⁻⁴ to 0.427 kg CO₂ equiv. These values are insignificant and are much lower than the values of the LCA evaluation study of cellulose nanofibrils production published by Arvidsson et al.⁶⁶

EC is the term used to describe a chemical's detrimental effects on ecosystems, including the living environment and the species that inhabit it. The permitted level of nanomaterial EC value falls between 3.0 and 8.0 CTUe/kg.⁵⁹ It is evident from our study's results that the EC values of both methods are within a safe range. HT is another indicator that measures the extent to which harmful substances have a detrimental impact on human health. This measure displays the number of possible illnesses (cases) per unit of emission (i.e., kilograms of pollutant). For example, several studies have shown that some chemical substances, such as dioxin or benzene, might induce cancer or other serious illnesses,^{67,68} contributing to elevated CTUe. In both PEG/SFPs-CTX formulation processes, the HT values range from 1.21.10⁻¹⁰ to 3.66.10⁻⁸, which can be seen to be very low. As a result, it can be concluded that all of the processes of this study are safe for humans. OD is used to refer to the weakening and thinning of the ozone layer in the stratosphere, mainly caused by chemicals emitted by humans, such as chlorofluorocarbon (CFC). The ozone layer plays an important role because it acts as a shield to protect the earth, protecting the ecosystems from the harmful UV radiations.⁶⁹ The reference unit kg CFC11 equiv is often used in LCA to demonstrate the potential OD potential of a research object compared to CFC-11. According to the literature, the baseline level of OD potential of CFC-11 is 1.0.⁷⁰ Comparing with our results, the OD impact of the co-condensation method is 2.12.10⁻⁸ kg CFC11 equiv, and that of the adsorption method is 1.03.10⁻⁸ kg CFC11 equiv. These values are much smaller than the baseline level of 1.0 of CFC-11, so both processes are not potential OD contributors. All other impacts also exhibit low values and do not adversely affect the environment.

Overall, both PEG/SFPs-CTX formulation processes are environmentally friendly and did not cause significant effects on the environment. The adsorption method is "greener" than the co-condensation method, with lower impact values, due to the limitation use of ethanol in the formulation process.

4. CONCLUSIONS

This study effectively formulated SFPs and PEG/SFPs for the oral delivery of antibiotic CTX using the eco-friendly and green processes of co-condensation and adsorption. The particles possessed spherical shape, nanosize with narrow size distribution, negative charge, and adequate drug entrapment efficiency of ~50%. Interestingly, depending on the formulation process, the CTX could be loaded in the particles in

either crystalline or amorphous form, which consequently affected its release rate in the gastrointestinal tract. These alterations are favorable for oral delivery of CTX. In-depth docking and MD simulation revealed that the PEG/SFPs-CTX exhibited high stability and strong interactions through hydrogen bonds, van der Waals forces, and π - π interactions, and CTX was protected and controlled released in physiological environments. Moreover, LCA analysis showed that both formulation methods were environmentally friendly, with limited impacts on the ecosystem, and the adsorption method was "greener" than the co-condensation method. These data could provide insights for future research on the formulations of SFPs as drug delivery systems.


■ ASSOCIATED CONTENT

Data Availability Statement


All data underlying the findings described in their manuscript are fully available without restriction.

■ AUTHOR INFORMATION

Corresponding Author

Bui Thi Phuong Thuy – Faculty of Fundamental Sciences, Van Lang University, Ho Chi Minh City 70000, Vietnam;  orcid.org/0000-0001-5487-414X; Email: thuy.btp@vlu.edu.vn

Authors

Duy Toan Pham – Department of Health Sciences, College of Natural Sciences, Can Tho University, Can Tho 900000, Vietnam;  orcid.org/0000-0002-8693-3367

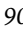
Thi Truc Dao Le – Department of Health Sciences, College of Natural Sciences, Can Tho University, Can Tho 900000, Vietnam

Ngoc Yen Nguyen – Department of Health Sciences, College of Natural Sciences, Can Tho University, Can Tho 900000, Vietnam

Chong Kim Thien Duc – Department of Health Sciences, College of Natural Sciences, Can Tho University, Can Tho 900000, Vietnam

Nguyen Trong Tuan – Department of Health Sciences, College of Natural Sciences, Can Tho University, Can Tho 900000, Vietnam

Huynh Vu Thanh Luong – Faculty of Chemical Engineering, College of Engineering, Can Tho University, Can Tho 900000, Vietnam

Quyen Thi Bich Tran – Faculty of Chemical Engineering, College of Engineering, Can Tho University, Can Tho 900000, Vietnam;  orcid.org/0000-0002-9304-5544

Manh Quan Nguyen – Department of Analytical Chemistry-Drug Quality Control, Faculty of Pharmacy, Can Tho University of Medicine and Pharmacy, Can Tho 900000, Vietnam

Complete contact information is available at:

<https://pubs.acs.org/10.1021/acsomega.5c01089>

Author Contributions

Conceptualization: D.T.P., B.T.P.T.; methodology: D.T.P., T.T.D.L., N.Y.N., C.K.T.D., N.T.T., H.V.T.L., Q.T.B.T., M.Q.N., B.T.P.T.; investigation: D.T.P., T.T.D.L., N.Y.N., C.K.T.D., N.T.T., H.V.T.L., Q.T.B.T., M.Q.N.; data curation: D.T.P., T.T.D.L., N.Y.N., C.K.T.D., N.T.T., H.V.T.L., Q.T.B.T., M.Q.N.; validation: D.T.P., B.T.P.T.; project administration: B.T.P.T.; resource: B.T.P.T.; writing—original

draft: D.T.P., B.T.P.T.; writing—review and editing: D.T.P., T.T.D.L., N.Y.N., C.K.T.D., N.T.T., H.V.T.L., Q.T.B.T., M.Q.N., B.T.P.T. All authors have read and agreed to the published version of the manuscript.

Notes

The authors declare no competing financial interest.

ACKNOWLEDGMENTS

The authors thank Can Tho University, Can Tho University of Medicine and Pharmacy, and Van Lang University for the helpful support.

REFERENCES

- (1) Alqahtani, M. S.; Kazi, M.; Alsenaidy, M. A.; Ahmad, M. Z.; et al. Advances in oral drug delivery. *Front. Pharmacol.* **2021**, *12*, 1–21.
- (2) Islam, M. S.; Reineke, J.; Kaushik, R.; Woyengo, T.; Baride, A.; Alqahtani, M. S.; Perumal, O. Bioadhesive Food Protein Nanoparticles as Pediatric Oral Drug Delivery System. *ACS Appl. Mater. Interfaces* **2019**, *11*, 18062–18073.
- (3) Wolie, Z. T.; Roberts, J. A.; Gilchrist, M.; McCarthy, K.; Sime, F. B. Current practices and challenges of outpatient parenteral antimicrobial therapy: a narrative review. *J. Antimicrob. Chemother.* **2024**, *79*, 2083–2102.
- (4) Boyd, B. J.; Bergström, C. A. S.; Vinarov, Z.; Kuentz, M.; Brouwers, J.; Augustijns, P.; Brandl, M.; Bernkop-Schnürch, A.; Shrestha, N.; Prétat, V.; Müllertz, A.; Bauer-Brandl, A.; Jannin, V. Successful oral delivery of poorly water-soluble drugs both depends on the intraluminal behavior of drugs and of appropriate advanced drug delivery systems. *Eur. J. Pharm. Sci.* **2019**, *137*, No. 104967.
- (5) Kohli, K.; Chopra, S.; Dhar, D.; Arora, S.; Khar, R. K. Self-emulsifying drug delivery systems: An approach to enhance oral bioavailability. *Drug Discovery Today* **2010**, *15*, 958–965.
- (6) Mathur, A. B.; Gupta, V. Silk Fibroin-Derived Nanoparticles for Biomedical Applications. *Nanomedicine* **2010**, *5*, 807–820.
- (7) Pham, D. T.; Tiyafoonchai, W. Fibroin nanoparticles: a promising drug delivery system. *Drug Delivery* **2020**, *27*, 431–448.
- (8) Ki, C. S.; Park, Y. H.; Jin, H. J. Silk protein as a fascinating biomedical polymer: Structural fundamentals and applications. *Macromol. Res.* **2009**, *17*, 935–942.
- (9) Pham, D. T.; Saelim, N.; Tiyafoonchai, W. Crosslinked fibroin nanoparticles using EDC or PEI for drug delivery: physicochemical properties, crystallinity and structure. *J. Mater. Sci.* **2018**, *53*, 14087–14103.
- (10) Pham, D. T.; Saelim, N.; Tiyafoonchai, W. Paclitaxel loaded EDC-crosslinked fibroin nanoparticles: a potential approach for colon cancer treatment. *Drug Delivery Transl. Res.* **2020**, *10*, 413.
- (11) Chomchalao, P.; Nimtrakul, P.; Pham, D. T.; Tiyafoonchai, W. Development of amphotericin B-loaded fibroin nanoparticles: a novel approach for topical ocular application. *J. Mater. Sci.* **2020**, *55*, 5268–5279.
- (12) Pham, D. T.; Nguyen, T. L.; Nguyen, T. T. L.; Nguyen, T. T. P.; Ho, T. K.; Nguyen, N. Y.; Tran, V. D.; Ha, T. K. Q. Polyethylenimine-functionalized fibroin nanoparticles as a potential oral delivery system for BCS class-IV drugs, a case study of furosemide. *J. Mater. Sci.* **2023**, *58*, 9660–9674.
- (13) Pham, D. T.; Ha, T. K. Q.; Nguyen, M. Q.; Tran, V. D.; Nguyen, V. B.; Quyen, T. T. B. Silk fibroin nanoparticles as a versatile oral delivery system for drugs of different biopharmaceutics classification system (BCS) classes: A comprehensive comparison. *J. Mater. Res.* **2022**, *37*, 4169–4181.
- (14) Pham, D. T.; Huynh, Q. C.; Lieu, R.; Nguyen, V. B.; Tran, V. D.; Thuy, B. T. P. Controlled-Release Wedelia trilobata L. Flower Extract Loaded Fibroin Microparticles as Potential Anti-Aging Preparations for Cosmetic Trade Commercialization. *Clinical, Cosmetic and Investigational Dermatology* **2023**, *16*, 1109–1121.
- (15) Pham, D. T.; Nguyen, D. X. T.; Lieu, R.; Huynh, Q. C.; Nguyen, N. Y.; Quyen, T. T. B.; Tran, V. D. Silk nanoparticles for the protection and delivery of guava leaf (*Psidium guajava* L.) extract for cosmetic industry, a new approach for an old herb. *Drug Delivery* **2023**, *30*, 2168793.
- (16) Jia, L.; Guo, L.; Zhu, J.; Ma, Y. Stability and cytocompatibility of silk fibroin-capped gold nanoparticles. *Materials Science and Engineering C* **2014**, *43*, 231–236.
- (17) Pham, D. T.; Tetyczka, C.; Hartl, S.; Absenger-Novak, M.; Fröhlich, E.; Tiyafoonchai, W.; Roblegg, E. Comprehensive investigations of fibroin and poly(ethylenimine) functionalized fibroin nanoparticles for ulcerative colitis treatment. *Journal of Drug Delivery Science and Technology* **2020**, *57*, No. 101484.
- (18) Di, K. N.; Ha, P. T. M.; Nguyen, N. P.; Nguyen, N. Y.; Truong, T. C.; Nguyen, T. T. V.; Truong, Q.-K.; Nguyen, M. Q.; Pham, D. T. Enhanced Anti-inflammatory Effects of Diclofenac Delivered Orally via Polyvinylpyrrolidone K30/Silk Fibroin Nanoparticles in a Murine Model of Carrageenan-Induced Paw Edema. *ChemMedChem* **2024**, No. e202400760.
- (19) Hudită, A.; Radu, I. C.; Zaharia, C.; Ion, A. C.; Ginghină, O.; Gălăteanu, B.; Mărutescu, L.; Grama, F.; Tsatsakis, A.; Gurevich, L.; Costache, M. Bio- and Hemo-Compatible Silk Fibroin PEGylated Nanocarriers for 5-Fluorouracil Chemotherapy in Colorectal Cancer. *In Vitro Studies, Pharmaceuticals* **2021**, *13*, 755.
- (20) Totten, J. D.; Wongpinyochit, T.; Carrola, J.; Duarte, I. F.; Seib, F. P. PEGylation-Dependent Metabolic Rewiring of Macrophages with Silk Fibroin Nanoparticles. *ACS Appl. Mater. Interfaces* **2019**, *11*, 14515–14525.
- (21) Jeshvaghani, P. A.; Pourmadadi, M.; Yazdian, F.; Rashedi, H.; Khoshmaram, K.; Nigjeh, M. N. Synthesis and characterization of a novel, pH-responsive sustained release nanocarrier using polyethylene glycol, graphene oxide, and natural silk fibroin protein by a green nano emulsification method to enhance cancer treatment. *Int. J. Biol. Macromol.* **2023**, *226*, 1100–1115.
- (22) Liu, X.; Luo, H.; Niu, L.; Feng, Y.; Pan, P.; Yang, J.; Li, M. Cleavable Poly(Ethylene Glycol) Branched Chain-Modified Anthraene Pernyi Silk Fibroin as A Gene Delivery Carrier. *Nanomedicine* **2021**, *16*, 839–853.
- (23) Parray, Z. A.; Hassan, M. I.; Ahmad, F.; Islam, A. Amphiphilic nature of polyethylene glycols and their role in medical research. *Polym. Test.* **2020**, *82*, No. 106316.
- (24) D'souza, A. A.; Shegokar, R. Polyethylene glycol (PEG): a versatile polymer for pharmaceutical applications. *Expert Opinion on Drug Delivery* **2016**, *13*, 1257–1275.
- (25) Shi, L.; Zhang, J.; Zhao, M.; Tang, S.; Cheng, X.; Zhang, W.; Li, W.; Liu, X.; Peng, H.; Wang, Q. Effects of polyethylene glycol on the surface of nanoparticles for targeted drug delivery. *Nanoscale* **2021**, *13*, 10748–10764.
- (26) Barz, M.; Luxenhofer, R.; Zentel, R.; Vicent, M. J. Overcoming the PEG-addiction: Well-defined alternatives to PEG, from structure-property relationships to better defined therapeutics. *Polym. Chem.* **2011**, *2*, 1900–1918.
- (27) Nosova, A. S.; Koloskova, O. O.; Nikonova, A. A.; Simonova, V. A.; Smirnov, V. V.; Kudlay, D.; Khaitov, M. R. Diversity of PEGylation methods of liposomes and their influence on RNA delivery. *MedChemComm* **2019**, *10*, 369–377.
- (28) Sharma, B.; Chalikwar, R.; Bhalerao, S.; Gondane, A. A.; Pawar, D.; Sharma, A. Cefotaxime Versus Ceftriaxone: A Comprehensive Comparative Review. *Cureus* **2024**, *16*, No. e69146.
- (29) Muhtudi, F. J.; Hassan, M. M. A. Cefotaxime. *Anal. Profiles Drug Subst.* **1982**, *11*, 139.
- (30) Pacifici, G. M.; Marchini, G. Clinical pharmacology of cefotaxime in neonates and infants: Effects and pharmacokinetics. *Int. J. Pediatr.* **2017**, *5*, 6111–6138.
- (31) Fu, K. P.; Neu, H. C. Antibacterial activity of ceftizoxime, a β -lactamase-stable cephalosporin. *Antimicrob. Agents Chemother.* **1980**, *17*, 583–590.
- (32) Mitsushashi, S.; Inoue, M.; Masayoshi, S. Antibacterial activity of cefotaxime. *J. Antimicrob. Chemother.* **1980**, *6*, 37–46.
- (33) Guerra Valero, Y. C.; Dorofaeff, T.; Coulthard, M. G.; Sparkes, L.; Lipman, J.; Wallis, S. C.; Roberts, J. A.; Parker, S. L. Optimal

dosing of cefotaxime and desacetylcefotaxime for critically ill paediatric patients. Can we use microsampling? *J. Antimicrob. Chemother.* **2022**, *77*, 2227–2237.

(34) Fabre, H.; Eddine, N. H.; Berge, G. Degradation kinetics in aqueous solution of cefotaxime sodium, a third-generation cephalosporin. *J. Pharm. Sci.* **1984**, *73*, 611–618.

(35) He, Y.-X.; Zhang, N.-N.; Li, W.-F.; Jia, N.; Chen, B.-Y.; Zhou, K.; Zhang, J.; Chen, Y.; Zhou, C.-Z. N-Terminal Domain of *Bombyx mori* Fibroin Mediates the Assembly of Silk in Response to pH Decrease. *J. Mol. Biol.* **2012**, *418*, 197–207.

(36) Morris, G. M.; Lim-Wilby, M. Molecular docking. *Methods Mol. Biol.* **2008**, *443*, 365–382.

(37) Mouli, H. M. C.; Harini, D.; Shaikh, N.; Khemchandani, R.; Shreya, S.; Jana, A.; Samanthula, G. In silico characterization of indole-substituted densely functionalized pyrrole against breast cancer: Integrating DFT, molecular docking, MD simulations, and ADME analysis. *J. Mol. Struct.* **2025**, *1328*, No. 141375.

(38) Park, S.-J.; Kern, N.; Brown, T.; Lee, J.; Im, W. CHARMM-GUI PDB Manipulator: Various PDB Structural Modifications for Biomolecular Modeling and Simulation. *J. Mol. Biol.* **2023**, *435*, No. 167995.

(39) Kumah, E. A.; Fopa, R. D.; Harati, S.; Boadu, P.; Zohoori, F. V.; Pak, T. Human and environmental impacts of nanoparticles: a scoping review of the current literature. *BMC Public Health* **2023**, *23*, 1059.

(40) Wani, S. U. D.; Ali, M.; Masoodi, M. H.; Khan, N. A.; Zargar, M. I.; Hassan, R.; Mir, S. A.; Gautam, S. P.; Gangadharappa, H. V.; Osmani, R. A. M. A review on nanoparticles categorization, characterization and applications in drug delivery systems. *Vib. Spectrosc.* **2022**, *121*, No. 103407.

(41) Curran, M. A. Life Cycle Assessment: a review of the methodology and its application to sustainability. *Current Opinion in Chemical Engineering* **2013**, *2*, 273–277.

(42) Nguyen, N. Y.; Nguyen, T. N. P.; Huyen, N. N.; Tran, V. D.; Quyen, T. T. B.; Luong, H. V. T.; Pham, D. T. Onto the differences in formulating micro-/nanoparticulate drug delivery system from Thai silk and Vietnamese silk: A critical comparison. *Heliyon* **2023**, *9*, No. e16966.

(43) Thao, N. T. P.; Nguyen, N. Y.; Co, V. B.; Thanh, L. H. V.; Nguyen, M. Q.; Pan-On, S.; Pham, D. T. Formulations of poly(vinyl alcohol) functionalized silk fibroin nanoparticles for the oral delivery of zwitterionic ciprofloxacin. *PLoS One* **2024**, *19*, No. e0306140.

(44) Pham, D. T.; Nguyen, D. X. T.; Nguyen, N. Y.; Nguyen, T. T. L.; Nguyen, T. Q. C.; Tu, A. V. T.; Nguyen, N. H.; Thuy, B. T. P. Development of pH-responsive Eudragit S100-functionalized silk fibroin nanoparticles as a prospective drug delivery system. *PLoS One* **2024**, *19*, No. e0303177.

(45) Nguyen, N. N. T.; Duong, X. C.; Nguyen, K. N.; Nguyen, T. N. V.; Nguyen, T. T. D.; Nguyen, T. T. T.; Yen Le, T. T.; Tu Le, T. C.; Pham, D. T. Development and in-vitro/in-vivo evaluation of film-coated tablets containing *Azadirachta indica* A. Juss leaf extracts for diabetes treatment. *J. Appl. Pharm. Sci.* **2022**, *13*, 193–200.

(46) Ohanyan, N.; Abelyan, N.; Manukyan, A.; Hayrapetyan, V.; Chailyan, S.; Tiratsuyan, S.; Danielyan, K. Tannin–Albumin Particles as Stable Carriers of Medicines. *Nanomedicine* **2024**, *19*, 689–708.

(47) Khanna, N.; Wadhwa, J.; Pitroda, A.; Shah, P.; Schoop, J.; Sarikaya, M. Life cycle assessment of environmentally friendly initiatives for sustainable machining: A short review of current knowledge and a case study. *Sustainable Materials and Technologies* **2022**, *32*, No. e00413.

(48) El Chami, D.; Santagata, R.; Moretti, S.; Moreschi, L.; Del Borghi, A.; Gallo, M. A Life Cycle Assessment to Evaluate the Environmental Benefits of Applying the Circular Economy Model to the Fertiliser Sector. *Sustainability* **2023**, *15*, 15468.

(49) Pham, D. T.; Saelim, N.; Tiyafoonchai, W. Alpha mangostin loaded crosslinked silk fibroin-based nanoparticles for cancer chemotherapy. *Colloids Surf., B* **2019**, *181*, 705–713.

(50) Pham, D. T.; Saelim, N.; Tiyafoonchai, W. Design of experiments model for the optimization of silk fibroin based

nanoparticles. *International Journal of Applied Pharmaceutics* **2018**, *10*, 195–201.

(51) Pham, D. T.; Tiyafoonchai, W. Fibroin nanoparticles: a promising drug delivery system. *Drug Delivery* **2020**, *27*, 431–448.

(52) Polu, A. R.; Kumar, R. Impedance Spectroscopy and FTIR Studies of PEG - Based Polymer Electrolytes. *J. Chem.* **2011**, *8* (1), 347–353.

(53) Al Hagbani, T.; Rizvi, S. M. D.; Hussain, T.; Mehmood, K.; Rafi, Z.; Moin, A.; Abu Lila, A. S.; Alshammari, F.; Khafagy, E.-S.; Rahamathulla, M.; Abdallah, M. H. Cefotaxime Mediated Synthesis of Gold Nanoparticles: Characterization and Antibacterial Activity. *Polymers* **2022**, *14*, 1–12.

(54) Markad, M. H.; Mankar, S. D. Solubility Enhancement of Poorly Water Soluble Drugs: A review. *Asian Journal of Research in Pharmaceutical Sciences* **2022**, *5*, 231–238.

(55) Paarakh, M. P.; Jose, P. A.; Setty, C. Release Kinetics – Concepts and Applications. *Int. J. Pharm. Res. Technol.* **2019**, *8*, 12.

(56) Nguyen, N. N. T.; Pham, D. T.; Nguyen, D. T.; Trinh, T. T. L. Bilayer tablets with sustained-release metformin and immediate-release sitagliptin: preparation and in vitro/in vivo evaluation. *Journal of Pharmaceutical Investigation* **2021**, *51*, 579–586.

(57) Permanadewi, I.; Kumoro, A. C.; Wardhani, D. H.; Aryanti, N. Modelling of controlled drug release in gastrointestinal tract simulation. *J. Phys.: Conf. Ser.* **2019**, *1295*, No. 012063.

(58) Tran, D. P.; Lam, V. T.; Tran, T. L.; Nguyen, T. N. S.; Thi Tran, H. T. In silico study of *Bombyx mori* fibroin enhancement by graphene in acidic environment. *Phys. Chem. Chem. Phys.* **2018**, *20*, 19240–19249.

(59) Nizam, N. U. M.; Hanafiah, M. M.; Woon, K. S. A Content Review of Life Cycle Assessment of Nanomaterials: Current Practices, Challenges, and Future Prospects. *Nanomaterials (Basel)* **2021**, *11*, 3324.

(60) Weyell, P.; Kurland, H.-D.; Hülser, T.; Grabow, J.; Müller, F. A.; Kralisch, D. Risk and life cycle assessment of nanoparticles for medical applications prepared using safe- and benign-by-design gas-phase syntheses. *Green Chem.* **2020**, *22*, 814–827.

(61) del Pilar Rodríguez-Rojas, M.; Bustos-Terrones, V.; Díaz-Cárdenas, M. Y.; Vázquez-Vélez, E.; Martínez, H. Life Cycle Assessment of Green Synthesis of TiO₂ Nanoparticles vs. Chemical Synthesis. *Sustainability* **2024**, *16*, 7751.

(62) Oniha, M. I.; Oyejide, S. O., Life Cycle Assessment of Nanoparticles, In: Isibor, P. O.; Devi, G.; Enuneku, A. A. (Eds.), *Environmental Nanotoxicology: Combatting the Minute Contaminants*; Springer Nature: Switzerland, Cham, 2024; pp 317–324. .

(63) Hengjie, T.; Das, S. K.; Zainee, N. F. A.; Yana, R.; Rozaimi, M. Ocean Acidification and Aquacultured Seaweeds: Progress and Knowledge Gaps. *Journal of Marine Science and Engineering* **2023**, *11*, 78.

(64) Yang, B.; Zhang, H.; Ke, W.; Jiang, J.; Xiao, Y.; Tian, J.; Zhu, X.; Zong, L.; Fang, W. Effect of Soil Acidification on the Production of Se-Rich Tea. *Plants* **2023**, *12*, 2882.

(65) Picano, E.; Mangia, C.; D'Andrea, A. Climate Change, Carbon Dioxide Emissions, and Medical Imaging Contribution, *Journal of Clinical Medicine* **2023**, *12*, 215.

(66) Arvidsson, R.; Nguyen, D.; Svanström, M. Life Cycle Assessment of Cellulose Nanofibrils Production by Mechanical Treatment and Two Different Pretreatment Processes. *Environ. Sci. Technol.* **2015**, *49*, 6881–6890.

(67) Piwarski, S. A.; Salisbury, T. B. The effects of environmental aryl hydrocarbon receptor ligands on signaling and cell metabolism in cancer. *Biochem. Pharmacol.* **2023**, *216*, No. 115771.

(68) Chiavarini, M.; Rosignoli, P.; Sorbara, B.; Giachetta, I.; Fabiani, R. Benzene Exposure and Lung Cancer Risk: A Systematic Review and Meta-Analysis of Human Studies. *International Journal of Environmental Research and Public Health* **2024**, *21*, 205.

(69) Neale, R. E.; Barnes, P. W.; Robson, T. M.; Neale, P. J.; Williamson, C. E.; Zepp, R. G.; Wilson, S. R.; Madronich, S.; Andrad, A. L.; Heikkilä, A. M.; Bernhard, G. H.; Bais, A. F.; Aucamp, P. J.; Banaszak, A. T.; Bornman, J. F.; Bruckman, L. S.; Byrne, S. N.;

Foereid, B.; Häder, D.-P.; Hollestein, L. M.; Hou, W.-C.; Hylander, S.; Jansen, M. A. K.; Klekociuk, A. R.; Liley, J. B.; Longstreth, J.; Lucas, R. M.; Martinez-Abaigar, J.; McNeill, K.; Olsen, C. M.; Pandey, K. K.; Rhodes, L. E.; Robinson, S. A.; Rose, K. C.; Schikowski, T.; Solomon, K. R.; Sulzberger, B.; Ukpebor, J. E.; Wang, Q.-W.; Wängberg, S.-Å.; White, C. C.; Yazar, S.; Young, A. R.; Young, P. J.; Zhu, L.; Zhu, M. Environmental effects of stratospheric ozone depletion, UV radiation, and interactions with climate change: UNEP Environmental Effects Assessment Panel, Update 2020. *Photochem. Photobiol. Sci.* **2021**, *20*, 1–67.

(70) Wuebbles, D. J., Ozone depletion and related topics: Ozone Depletion Potentials, In: North, G. R.; Pyle, J.; Zhang, F. (Eds.), *Encyclopedia of Atmospheric Sciences: Second edition*; Academic Press: Oxford, 2015: pp 364–369. .